Ultrafast Electron-Electron Scattering in Metallic Phase of 2H-$NbSe_2$ Probed by High Harmonic Generation

K. S. Takeda, K. Uchida,* K. Nagai, S. Kusaba, S. Takahashi, and K. Tanaka†
Department of Physics, Graduate School of Science, Kyoto University, Kyoto 606-8502, Japan

(Received 12 February 2023; revised 31 December 2023; accepted 19 March 2024; published 1 May 2024)

Electron-electron scattering on the order of a few to tens of femtoseconds plays a crucial role in the ultrafast electron dynamics of conventional metals. When mid-infrared light is used for driving and the period of light field is comparable to the scattering time in metals, unique light-driven states and nonlinear optical responses associated with the scattering process are expected to occur. Here, we use high-harmonics spectroscopy to investigate the effect of electron-electron scattering on the electron dynamics in thin film 2H-$NbSe_2$ driven by a mid-infrared field. We observed odd-order high harmonics up to 9th order as well as a broadband emission from hot electrons in the energy range from 1.5 to 4.0 eV. The electron-electron scattering time in 2H-$NbSe_2$ was estimated from the broadband emission to be almost the same as the period of the mid-infrared light field. A comparison between experimental results and a numerical calculation reveals that competition and cooperation between the driving and scattering enhances the nonperturbative behavior of high harmonics in metals, causing a highly nonequilibrium electronic state corresponding to several thousand Kelvin.

DOI: 10.1103/PhysRevLett.132.186901

Electron dynamics driven by an intense light field induce novel nonlinear optical phenomena and sometimes result in nontrivial light-induced phase transitions in solids [1–3]. An understanding of the dynamics is crucial to not only fundamental optical science but also the development of applications such as ultrafast manipulation of material properties and femtosecond-laser processing [4–7]. In dilute atomic or molecular systems, where strong-field physics have been intensively studied, electron motion is fully ballistic and coherent without any scattering. On the other hand, in solids, scattering by other electrons or other degrees of freedom occurs under driving. When the typical scattering timescale is longer than the period of the driving field, the electron motion can be regarded as coherent and ballistic, as in atoms [2,8–11]. On the other hand, when the typical scattering time is shorter than the driving period, scattering disrupts the ballistic electron motion (called a drift-diffusive regime) [12] and prevents the formation of nonequilibrium states. In the intermediate regime where the scattering time is comparable to the driving-field period [13], the interplay between driving and scattering causes electrons to absorb a huge amount of energy from the driving field and the electron distribution moves far from the equilibrium one. Nonlinear optical response reflecting a scattering process unique to solids is also expected to occur in this regime. So far, however, only a few experimental studies on ultrafast electron dynamics in solids under driving fields have considered the effects of scattering and dissipation processes [14–18].

Metals under a strong mid-infrared (MIR) driving field provide a fascinating playground for studying light-driven states and nonlinear optical processes associated with scattering. The electron-electron (e–e) scattering time in metals is typically about 1–10 fs [19], and this value is comparable to the period of MIR light, i.e., the intermediate regime discussed above. Moreover, in metals, we can assume the simplest condition, i.e., intraband motion of electrons within a single band. This contrasts with the circumstances of semiconductors and semimetals, where electrons in principle move across multiple bands and their dynamics are quite complicated. However, so far, extremely nonlinear optical processes such as high order harmonic generation (HHG) have mainly been studied in semiconductors and insulators [20,21], whereas only a few studies have targeted metals [22]. This is because the electric field is strongly screened inside metals, making it difficult to apply a strong MIR electric field to electrons in bulk metals. It is still a challenging problem to observe the electron dynamics in the intermediate regime.

In this study, we performed nonlinear emission measurements in a thin film of the metallic phase of 2H-$NbSe_2$ driven by intense MIR light in order to clarify the electron dynamics with ultrafast dissipation under driving. We observed high harmonics from the 5th to 9th order as well

as a broadband emission from 1.5 to 4.0 eV that has not been observed before in semiconductors and insulators. We attribute the nonlinear broadband emission to incoherent thermal radiation from hot electrons reaching 4000 K. These results indicate that the electrons in the metal are driven in reciprocal space with a large amplitude and strongly scattered at the same time, forming a high-temperature electron distribution immediately after driving. Our numerical results reveal that the e-e scattering time is comparable to the period of the driving field and that cooperation between driving and scattering leads to unique extreme nonlinear optical properties in metals.

The target sample was a thin film of metallic 2H-$NbSe_2$. Since 2H-$NbSe_2$ is a van der Waals layered material, we could obtain a sample with a thickness of 25 nm via the mechanical exfoliation method [23], which is sufficiently thinner than the penetration length of the excitation light (about 80 nm) [24]. Inside such a thin film, screening of the electric field, which occurs in bulk metals and often suppresses HHG signals [22], can be neglected. In addition, 2H-$NbSe_2$ has a simple quasi-two-dimensional band structure near the Fermi level, which can be easily put into a model [26,27]. We used a MIR pulse with a pulse width of 60 fs (full width at half maximum) and a center energy of $\hbar\Omega_{\mathrm{MIR}} = 0.26$ eV for excitation, and collected the nonlinear emission with transmission geometry by resolving its polarization state (see Supplemental Material [24] for the detailed experimental setup).

The upper panel of Fig. 1(a) shows typical emission spectra from 2H-$NbSe_2$ at an MIR intensity of 77 GW/cm^2 ($E_{\mathrm{MIR}} = 3.8$ MV/cm). One can see the peaks of the 5th, 7th, and 9th order harmonics in the emission that are polarized parallel to the MIR field (the blue solid line). There is no even-order harmonics, reflecting the centrosymmetric crystal structure of 2H-$NbSe_2$ [40]. Since the number of carriers generated through interband Zener tunneling in our experiment was estimated to be an order of magnitude smaller than that of the original free carriers [41,42], the high harmonics in 2H-$NbSe_2$ should have mainly come from the intraband motion of the original free carriers [22]. Ellipticity dependence of HHG yields also support the small contribution of interband transition in electron dynamics induced in our experimental condition [24]. Besides the high harmonics signals, a broadband emission was also observed in the photon energy range from 1.5 to 4.0 eV in both the parallel and perpendicular components.

Figure 1(b) shows the polarization state of the nonlinear emissions at 5th (red circles) and 7th (blue squares) harmonics energies and the broadband emission region (green triangles). The horizontal axis corresponds to the polarization direction of the excitation MIR light. The harmonic signals are well fitted with a cosine-squared function with a peak along the horizontal axis, indicating the polarization of the harmonic signals is parallel to that of

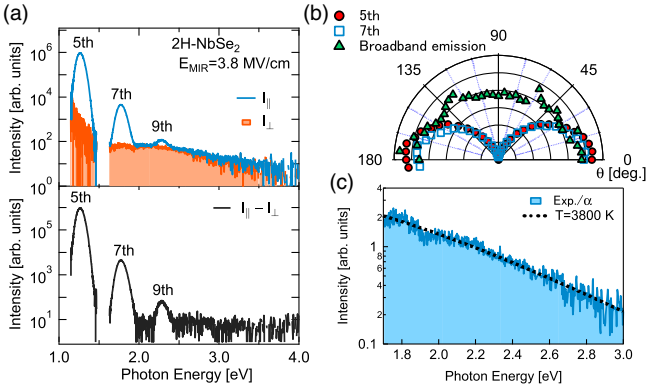

FIG. 1. (a) Typical HHG spectra in 2H-$NbSe_2$. Here, the MIR electric field inside the sample E_{MIR} is estimated to be 3.8 MV/cm. The blue line in the upper panel shows the emission polarized parallel to the MIR electric field. The orange shaded area shows the perpendicular component. The lower panel is the high harmonics spectrum obtained by subtracting the perpendicular component from the parallel component. Owing to the strong background signal by fundamental laser (1.55 eV), the spectrum between the 5th and 7th harmonics are noisy, and not shown for clarity. (b) Nonlinear emission intensity as a function of the transmission axis angle θ of the analyzer. Here, $\theta = 0°$ corresponds to the MIR electric field direction. Red circles and blue rectangles show the intensities corresponding to the 5th and 7th harmonics energy, respectively. Owing to the much stronger signal of the 5th and 7th harmonic emissions than the broadband emission, the contribution from the broadband emission in their polarization state is negligible. Green triangles show the broadband emission integrated over the region between 2.5 and 4.0 eV. Note that the polarization state at the 9th harmonics energy is not shown due to the low signal-to-noise ratio and comparable to broadband emission intensity. (c) Broadband emission spectrum divided by the absorptivity of the sample with $E_{\mathrm{MIR}} = 3.8$ MV/cm [24]. The dotted line represents the fitting result using the Planck distribution. The effective temperature estimated from the fitting is about 3800 K.

the incident MIR light. The broadband emission, on the other hand, is unpolarized. Hence, we can extract the high harmonic signal by subtracting the perpendicular component from the parallel component as shown in the bottom panel of Fig. 1(a).

So far, such a broadband emission has not been focused on in HHG measurements although there were several reports for semimetallic graphene and metallic carbon nanotubes [37,43]. Several studies reported that photoexcitation of metals and semimetals causes broadband emissions similar to our observation [44–47]. In these studies, the broadband emission was attributed to radiation originating from hot electrons that formed after electrons with high excess energy were created through near-infrared or visible light excitation of interband transitions. The broadband emission observed in our study should also originate from hot electrons. The difference between our experiment and the previous studies is that the hot electrons

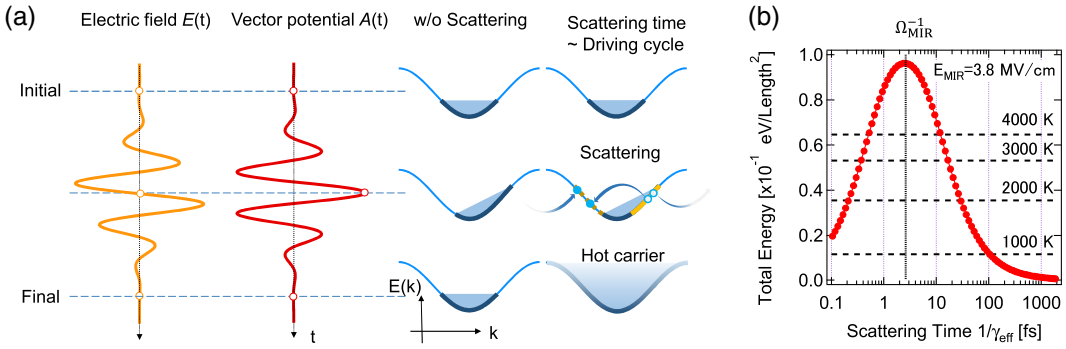

FIG. 2. (a) Schematic time evolution of the carrier distribution. Left panel shows the temporal profile of MIR electric field and the corresponding vector potential. Middle and right panels show the electron distribution in a one-dimensional cosine band at each time without and with the scattering effect, respectively. (b) Total energy of electron distribution of 2H-$NbSe_2$ after MIR-pulse excitation with $E_{\mathrm{MIR}} = 3.8$ MV/cm. The red line shows the total energy of the electron distribution that is asymptotic to the total energy before the excitation in the limit $\gamma_{\mathrm{eff}}^{-1} \to \infty$. Black dotted lines show the total energies of electrons for several temperatures.

formed through intense MIR driving of intraband electron motion, where the MIR photon energy is far below the band gap energy of 2H-$NbSe_2$ [24].

Assuming that the electron distribution after driving can be described by an effective temperature, the broadband emission spectrum divided by absorptivity can be fitted to the Planck distribution [Fig. 1(c)] [44]. The effective temperature estimated from this fit is 3800 K, and it is considered to be a transient value just after driving. This is because the effective electron temperature decreases over time through the electron-phonon coupling, and an electron distribution with a low effective temperature does not contribute to the broadband emission in the visible range [24]. The fact that the estimated temperature is far above the melting temperature of bulk 2H-$NbSe_2$ in vacuum also supports the conclusion that the broadband emission originates from a hot-electron subsystem before thermalizing with the lattice. The coexistence of high-order harmonics and a thermal emission in 2H-$NbSe_2$ suggests unique electron dynamics are at play in metals in the intermediate regime.

As mentioned above, the scattering process of the driven electrons should play a crucial role in the high-temperature electron distribution. Among the processes in metals, e-e scattering, which conserves the total energy of electrons, is the dominant contribution within the cycle of the driving field (16 fs). Figure 2(a) shows schematic diagrams of the energy transfer from a laser electric field to electrons in metals through intraband e-e scattering. When electrons follow the acceleration theorem without scattering, although their distribution is highly displaced during the driving, the final distribution after driving should be the same as the initial one, i.e., electrons absorb no energy from the driving field ["*w/o Scattering*" in Fig. 2(a)]. A previous study on HHG in metallic TiN film was performed in this regime [22]. In that study, visible light, whose period is shorter than the scattering time, was used for the excitation, and the most of the results could be accounted for by electron dynamics according to the acceleration theorem. On the other hand, when scattering is involved in the driven electron dynamics, the displaced electrons are scattered in reciprocal space, resulting in a high-temperature electron distribution after the driving field ["*Scattering time ~ Driving cycle*" in Fig. 2(a)].

To verify the above scenario, let us consider the Boltzmann transport equation [28]:

$$\frac{\partial f}{\partial t} - \frac{e}{\hbar}\boldsymbol{E}_{\mathrm{MIR}}(t)\cdot\nabla_{\boldsymbol{k}} f = \Sigma_{\mathrm{scatter}}, \tag{1}$$

where $f = f(\boldsymbol{k}, t)$ is the electron distribution function, $\boldsymbol{k}$ is the crystal momentum, $e(>0)$ is the electron charge, $\hbar$ is the Planck constant, and $E_{\mathrm{MIR}}(t)$ is the MIR electric field. For simplicity, we ignore the spatial diffusion term in the Boltzmann equation. In a simulation, we took $\boldsymbol{A}(t) = -\int_{-\infty}^{t} \mathrm{d}t' \boldsymbol{E}_{\mathrm{MIR}}(t')$ as the Gaussian pulse and used the experimental values for the pulse width and center frequency. The initial conditions were $f(\boldsymbol{k}, -\infty) = f_{\mathrm{F}}(\boldsymbol{k}, T = 300\ \mathrm{K})$, where $f_{\mathrm{F}}(\boldsymbol{k}, T)$ is the Fermi distribution function at temperature T. From $f(\boldsymbol{k}, t)$ one can calculate the electronic current as

$$\boldsymbol{j}(t) \propto -\int_{\mathrm{BZ}} d\boldsymbol{k} \frac{e}{\hbar}\frac{\partial \varepsilon(\boldsymbol{k})}{\partial \boldsymbol{k}} f(\boldsymbol{k}, t), \tag{2}$$

where $\varepsilon(\boldsymbol{k})$ is the band structure of 2H-$NbSe_2$. For simplicity, we used a band structure calculated from the two-dimensional tight binding model with three d orbitals [24–26]. From the calculated bands, we took the band that crossed the Fermi energy as $\varepsilon(\boldsymbol{k})$. The HHG spectrum was obtained from the Fourier transform of the current and given by $\boldsymbol{I}_{\mathrm{HH}}(\omega) \propto \omega |\tilde{\boldsymbol{j}}(\omega)|^2$.

To take e-e scattering into account, let us consider the simplest scattering process, i.e., backscattering, which causes a large modification to the electron distribution. We used the following phenomenological form, which is

extended from the one used in Refs. [30,24].

$$\Sigma_{\text{scatter}} = -\sum_{g} \gamma_g \{f(\boldsymbol{k}, t) - f(g\boldsymbol{k}, t)\}, \tag{3}$$

where g is the symmetric operation determined by the crystal symmetry of 2H-$NbSe_2$ (point group of D_{6h}) and γ_g is the scattering rate of each scattering path labeled by the symmetry operation g [24]. This form includes the Umklapp process and effectively describes the backscattering of electrons. A real system with a complicated band structure would have other scattering paths for electrons, which cannot be described by backscattering. Here, for simplicity, we will assume that only the backscattering channels are relevant in the timescale of interest (~10 fs) and that the scattering rate is the same for all paths in Eq. (3) ($\gamma_g = \gamma$). In this case, the effective scattering rate is given by $\gamma_{\text{eff}} = N\gamma$, where $N = 12$ is the number of symmetry operation in our model (see Supplemental Material [24] for the derivation of the effective scattering rate). We used the Fourier expansion method for the numerical calculation, and it enabled the electronic current and electron distribution to be calculated with high accuracy at a low computational cost [24].

Figure 2(c) shows the estimated total energy of electrons after driving as a function of the effective scattering time γ_{eff}^{-1} for $E_{\text{MIR}} = 3.8$ MV/cm [24]. Importantly, the total energy does not monotonically decrease as the scattering time increases and has a maximum value at $\gamma_{\text{eff}} = \Omega_{\text{MIR}}$. This is the result of cooperation and competition between the driving and scattering of electrons, which can be explained as follows. When the scattering is much longer than the cycle of the driving field, electrons follow the acceleration theorem and do not absorb energy much, as explained previously. On the other hand, when the scattering time is much shorter than the period, electrons are scattered immediately before they move a long way in reciprocal space; thus, the changes in the electron distribution are negligible. Note that this enhancement behavior is also expected when the driving field is weak, and thus is consistent with Drude model [24]. A highly nonequilibrium electronic distribution can be realized only in the intermediate regime where the scattering time is comparable to the cycle of the driving field. The estimated temperature of 3800 K for $E_{\text{MIR}} = 3.8$ MV/cm indicates that our experimental condition is indeed in the intermediate regime.

We estimated the typical scattering time in 2H-$NbSe_2$ by using the electron temperature value of 3800 K obtained from the broadband emission [24]. As shown in Fig. 2(c), there are two possible scattering times corresponding to an electron temperature of 3800 K. We chose the longer one ($\gamma_{\text{eff}}^{-1} = 13$ fs) since high harmonic emission was strongly suppressed for the shorter time in our simulation. The estimated value is consistent with typical e-e scattering times in metals [19] and comparable to the period of the MIR electric field ($2\pi/\Omega_{\text{MIR}} = 16$ fs). This indicates that our experimental conditions satisfy the intermediate regime discussed above.

To check whether the observed HHG results can be reproduced by our model using the scattering time estimated above ($\gamma_{\text{eff}}^{-1} = 13$ fs), we compared the experimental values with numerical HHG results. Figure 3(a) shows the experimental (red solid line) and calculated (gray dashed

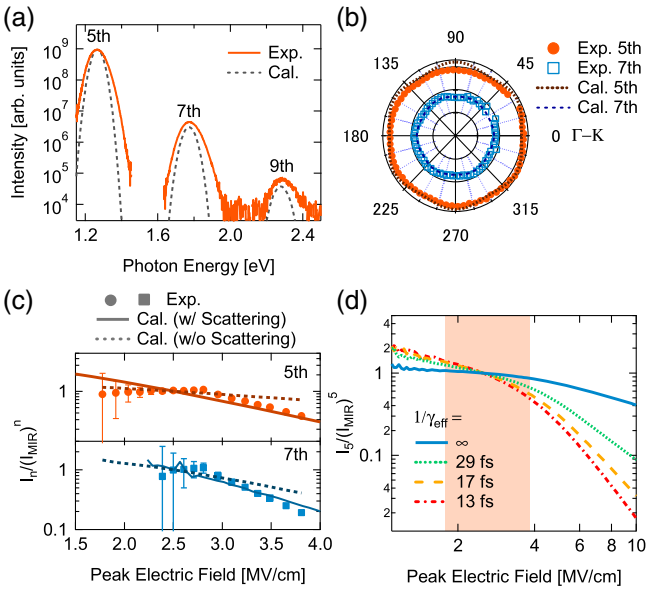

FIG. 3. Comparison of experimental and calculated results. (a) High harmonic spectra with $E_{\text{MIR}} = 3.8$ MV/cm. Orange solid and black dashed lines show the experimental and numerical results ($\gamma_{\text{eff}}^{-1} = 13$ fs), respectively. (b) Crystal orientation dependence of the 5th and 7th harmonics. Orange solid circles and blue open squares show the experimental results for the 5th and 7th harmonics, respectively. The brown dotted and dark-blue dashed lines show the corresponding numerical results ($E_{\text{MIR}} = 3.8$ MV/cm and $\gamma_{\text{eff}}^{-1} = 13$ fs). 0 degrees corresponds to the $\Gamma - K$ (zigzag) direction. For clarity, the intensity of the 7th harmonics is magnified. (c) Ratio of n th order harmonic intensity to the nth power of MIR intensity (I_n/I_{MIR}^n) as a function of MIR electric field. Symbols (circles and squares), solid, and dotted lines, respectively, show the experimental results, numerical results with and without scattering effect ($\gamma_{\text{eff}}^{-1} = 13$ fs and $=\infty$). The upper panel shows the 5th harmonic and lower panel shows the 7th. Here, all the data are normalized by the value at $E_{\text{MIR}} = 2.5$ MV/cm for clarity. (d) Ratio of the numerically simulated 5th harmonic intensity to the fifth power of MIR intensity (I_5/I_{MIR}^5) as a function of MIR electric field at certain scattering times. The blue solid line shows the results without the scattering effect. Green dotted, yellow dashed, and red dashed-dotted lines show the results with an effective scattering time γ_{eff}^{-1} of 29, 17, and 13 fs, respectively. Here, all the data are normalized by the value at $E_{\text{MIR}} = 2.5$ MV/cm. The shaded area shows the range of the MIR electric field in (c). In (b) and (c), the data corresponding to the 9th harmonics are not shown due to the low signal-to-noise ratio of the experiment.

line) high harmonics spectra with $E_{\mathrm{MIR}} = 3.8$ MV/cm. The numerical results reproduce the observed HHG spectrum, indicating that the scattering time estimated from the incoherent broadband emission is consistent with the scattering time in the coherent electron dynamics reflected in the observed high harmonic emission. In addition, the simulation also reproduces the almost isotropic crystal orientation dependence, which is in contrast to the rather anisotropic ones in several crystalline solids [24,48–55].

To clarify the nonperturbative nature of HHG in 2H-$NbSe_2$, we plot the ratio of the n th order harmonics intensity to the n th power of MIR intensity (I_n/I_{MIR}^n) as a function of MIR intensity in Fig. 3(c). This ratio should be constant for sufficiently weak MIR intensity because high harmonics signals obey a power law ($I_n \propto I_{\mathrm{MIR}}^n$) in the perturbative regime. When the light-matter interaction enters the nonperturbative regime as the MIR intensity increases, the ratio starts to depend on the MIR intensity, reflecting the electron dynamics unique to each material [20]. In our experiments, both the 5th and 7th harmonics show strong deviations from constant values, indicating a nonperturbative nonlinear optical process above 2.0 MV/cm. The numerical results for e-e scattering ($\gamma_{\mathrm{eff}}^{-1} = 13$ fs) reproduce the saturation seen in the experimental results, while the results without scattering are only weakly saturated. Overall, these results indicate that the scattering time estimated from the broadband emission is valid and that e–e scattering plays a crucial role in the nonperturbative nature of HHG in 2H-$NbSe_2$.

To investigate the effect of e-e scattering on the HHG process in more detail, we calculated the MIR intensity dependence of the high harmonics by changing the scattering time as shown in Fig. 3(d). The orange shaded area is the range of variation in the experiment. The deviation from perturbation theory monotonically increases with increasing MIR intensity and decreasing scattering time. This behavior can be understood as follows. When the MIR electric field is sufficiently weak, the change in the electron distribution from equilibrium is small, limiting the number of available scattering channels. As the MIR electric field increases, the electron distribution becomes more displaced from equilibrium, leading to an increase in available scattering channels. This increase in the scattering channels with the increase of MIR electric field suppresses the high harmonic signal originating from coherent electron motion. Since such a field-dependent scattering process should be universal in solids [13], the above scenario may substantially contribute to the nonperturbative nonlinearity of the optical response in a wide variety of systems, including metals and semiconductors.

In conclusion, we observed coherent high harmonic signals and an incoherent broadband emission induced by intense MIR driving in the metallic phase of 2H-$NbSe_2$. Since the incoherent broadband emission associated with HHG has not been observed in semiconductors and insulators, our observation indicates that the electron dynamics under strong MIR electric fields are unique to metals. We conclude that the broadband emission originates from hot electrons, whose effective temperature reaches around 4000 K. The numerical calculation including e–e scattering reproduced both the high harmonic spectrum and high electron temperature simply by tuning the e-e scattering time. The calculation revealed that energy absorption by electrons is enhanced in the intermediate regime owing to cooperation and competition between the driving and scattering processes. This enhancement condition is the cause of the unique nonlinear optical properties, such as scattering-induced nonperturbative nonlinearity, found in the HHG measurements. Our research proves that metals under a strong MIR field are suitable for studying the effect of ultrafast scattering on driven-electron systems in the intermediate regime. In general, the scattering process depends on the energy and momentum of electrons, and is prominent especially in quantum materials that host complicated electronic structure. This complicated scattering process may result in high harmonic emission and broadband emission highly depending on driving field strength and polarization. More precise measurements of field strength dependence and polarization dependence of nonlinear emission may help us uncover the nonequilibrium dynamics with dissipation in quantum materials.

K. U. thanks Dr. Taishi Nishihara and Mr. Katsuki Morimoto for fruitful discussion. This work was supported by Grants-in-Aid for Scientific Research (S) (Grants No. JP17H06124 and No. JP21H05017), JST ACCEL Grant (No. JPMJMI17F2). K. U. is thankful for a Grant-in-Aid for Young Scientists (Grant No. 19K14632), Grants-in-Aid for Scientific Research (C) (Grant No. JP 22K03484), and Grant-in-Aid for Challenging Research (Pioneering) (Grant No. 22K18322). S. K. was supported by MEXT Quantum Leap Flagship Program (No. JPMXS0118067634). K. N. was supported by a JSPS fellowship (Grant No. JP20J14428). S. T. was supported by JST SPRING (Grant No. JPMJSP2110).

*Corresponding author: uchida.kento.4z@kyoto-u.ac.jp
†Corresponding author: kochan@scphys.kyoto-u.ac.jp

[1] T. Oka and S. Kitamura, Floquet engineering of quantum materials, Annu. Rev. Condens. Matter Phys. **10**, 387 (2019).
[2] S. Y. Kruchinin, F. Krausz, and V. S. Yakovlev, Colloquium: Strong-field phenomena in periodic systems, Rev. Mod. Phys. **90**, 021002 (2018).
[3] A. de la Torre, D. M. Kennes, M. Claassen, S. Gerber, J. W. McIver, and M. A. Sentef, Colloquium: Nonthermal pathways to ultrafast control in quantum materials, Rev. Mod. Phys. **93**, 041002 (2021).
[4] M. Malinauskas, A. Žukauskas, S. Hasegawa, Y. Hayasaki, V. Mizeikis, R. Buividas, and S. Juodkazis, Ultrafast laser

processing of materials: from science to industry, Light Sci. Appl. **5**, e16133 (2016).
[5] F. Langer, C. P. Schmid, S. Schlauderer, M. Gmitra, J. Fabian, P. Nagler, C. Schüller, T. Korn, P. G. Hawkins, J. T. Steiner, U. Huttner, S. W. Koch, M. Kira, and R. Huber, Lightwave valleytronics in a monolayer of tungsten diselenide, Nature (London) **557**, 76 (2018).
[6] Á. Jiménez-Galán, R. E. F. Silva, O. Smirnova, and M. Ivanov, Lightwave control of topological properties in 2D materials for sub-cycle and non-resonant valley manipulation, Nat. Photonics **14**, 728 (2020).
[7] J.-Y. Shan, M. Ye, H. Chu, S. Lee, J.-G. Park, L. Balents, and D. Hsieh, Giant modulation of optical nonlinearity by Floquet engineering, Nature (London) **600**, 235 (2021).
[8] W. Kuehn, P. Gaal, K. Reimann, M. Woerner, T. Elsaesser, and R. Hey, Coherent ballistic motion of electrons in a periodic potential, Phys. Rev. Lett. **104**, 146602 (2010).
[9] F. Langer, M. Hohenleutner, C. P. Schmid, C. Poellmann, P. Nagler, T. Korn, C. Schüller, M. S. Sherwin, U. Huttner, J. T. Steiner, S. W. Koch, M. Kira, and R. Huber, Lightwave-driven quasiparticle collisions on a subcycle timescale, Nature (London) **533**, 225 (2016).
[10] T. Higuchi, C. Heide, K. Ullmann, H. B. Weber, and P. Hommelhoff, Light-field-driven currents in grapheme, Nature (London) **550**, 224 (2017).
[11] J. W. McIver, B. Schulte, F.-U. Stein, T. Matsuyama, G. Jotzu, G. Meier, and A. Cavalleri, Light-induced anomalous Hall effect in grapheme, Nat. Phys. **16**, 38 (2020).
[12] A. Jüngel, *Transport Equations for Semiconductors*, 1st ed. (Springer, Berlin, Heidelberg, 2009).
[13] J. B. Gunn, Instabilities of current in III–V semiconductors, IBM J. Res. Dev. **8**, 141 (1964).
[14] C. Heide, Y. Kobayashi, A. C. Johnson, F. Liu, T. F. Heinz, D. A. Reis, and Shambhu Ghimire, Probing electron-hole coherence in strongly driven 2D materials using high-harmonic generation, Optica **9**, 512 (2022).
[15] S. Xu, H. Zhang, J. Yu, Y. Han, Z. Wang, and J. Hu, Ultrafast modulation of a high harmonic generation in a bulk ZnO single crystal, Opt. Express **30**, 41350 (2022).
[16] K. Nagai, K. Uchida, S. Kusaba, T. Endo, Y. Miyata, and K. Tanaka, Effect of incoherent electron-hole pairs on high harmonic generation in atomically thin semiconductors, Phys. Rev. Res. **5**, 043130 (2023).
[17] G. Vampa, C. R. McDonald, G. Orlando, D. D. Klug, P. B. Corkum, and T. Brabec, Theoretical analysis of high-harmonic generation in solids, Phys. Rev. Lett. **113**, 073901 (2014).
[18] C-M. Wang, N. Tancogne-Dejean, M. Altarelli, A. Rubio, and S. A. Sato, Role of electron scattering on the high-order harmonic generation from solids, Phys. Rev. Res. **2**, 033333 (2020).
[19] N. W. Ashcroft and N. D. Mermin, *Solid State Physics* (Saunders College Publishing, Philadelphia, 1976).
[20] S. Ghimire and D. A. Reis, High-harmonic generation from solids, Nat. Phys. **15**, 10 (2019).
[21] J. Park, A. Subramani, S. Kim, and M. F. Ciappina, Recent trends in high-order harmonic generation in solids, Adv. Phys. **7**, 20032 (2022).
[22] A. Korobenko, S. Saha, A. T. K. Godfrey, M. Gertsvolf, A. Yu. Naumov, D. M. Villeneuve, A. Boltasseva, V. M. Shalaev, and P. B. Corkum, High-harmonic generation in metallic titanium nitride, Nat. Commun. **12**, 4981 (2021).
[23] K. Novoselov, A. K. Geim, S. V. Morozov, D. Jiang, Y. Zhang, S. Dubonos, I. Grigorieva, and A. A. Firsov, Electric field effect in atomically thin carbon films, Science **306**, 666 (2004).
[24] See Supplemental Material at http://link.aps.org/supplemental/10.1103/PhysRevLett.132.186901 for additional details, which includes Refs. [25–39].
[25] X. Xi, Z. Wang, W. Zhao, J.-H. Park, K. T. Law, H. Berger, L. Forró, J. Shan, and K. F. Mak, Ising pairing in superconducting NbSe2 atomic layers, Nat. Phys. **12**, 139 (2016).
[26] G.-B. Liu, W.-Y. Shan, Y. Yao, W. Yao, and D. Xiao, Three-band tight-binding model for monolayers of group-VIB transition metal dichalcogenides, Phys. Rev. B **88**, 085433 (2013).
[27] D. Möckli and M. Khodas, Robust parity-mixed superconductivity in disordered monolayer transition metal dichalcogenides, Phys. Rev. B **98**, 144518 (2018).
[28] L. P. Kadanoff and G. Baym, *Quantum Statistical Mechanics: Green's Function Methods in Equilibrium and Nonequilibrium Problems*, 1st ed. (W. A. Benjamin, Inc., New York, 1962).
[29] A. Jüngel, *Transport Equations for Semiconductors* 1st ed. (Springer, Berlin, Heidelberg, 2009).
[30] J. Reimann, S. Schlauderer, C. P. Schmid, F. Langer, S. Baierl, K. A. Kokh, O. E. Tereshchenko, A. Kimura, C. Lange, J. Güdde, U. Höfer, and R. Huber, Subcycle observation of lightwave-driven Dirac currents in a topological surface band, Nature (London) **562**, 396 (2018).
[31] M. Dressel and G. Grüner, *Electrodynamics of solids* (Cambridge University Press, Cambridge, England, 2002).
[32] R. Bachmann, H. C. Kirsch, and T. H. Geballe, Optical properties and superconductivity of $NbSe_2$, Solid State Commun. **9**, 57 (1971).
[33] W. Y. Liang, Reflectivity of MoS_2 and $NbSe_2$ (Interband transitions), J. Phys. C **4**, L378 (1971).
[34] G. Leveque, S. Robin-Kandare, L. Martin, and F. Pradal, Reflectivity of MoS_2 and $NbSe_2$ in the Extreme UV Range (20 to 70 eV), Phys. Status Solidi B **58**, K65 (1973).
[35] L. Martin, R. Mamy, A. Couget, and C. Raisin, Optical properties and collective excitations in MoS_2 and $NbSe_2$ in the 1.7 to 30 eV range, Phys. Status Solidi B **58**, 623 (1973).
[36] A. R. Beal, H. P. Hughes, and W. Y. Liang, The reflectivity spectra of some group VA transition metal dichalcogenides, J. Phys. C **8**, 4236 (1975).
[37] S. V. Dordevic, D. N. Basov, R. C. Dynes, and E. Bucher, Anisotropic electrodynamics of layered metal 2H-$NbSe_2$, Phys. Rev. B **64**, 161103(R) (2001).
[38] N. Yoshikawa, T. Tamaya, and K. Tanaka, High-harmonic generation in graphene enhanced by elliptically polarized light excitation. Science **356**, 736 (2017).
[39] S. A. Sato, H. Hirori, Y. Sanari, Y. Kanemitsu, and A. Rubio, High-order harmonic generation in graphene: Nonlinear coupling of intraband and interband transitions, Phys. Rev. B **103**, L041408 (2021).
[40] J. A. Wilson and A. D. Yoffe, The transition metal dichalcogenides discussion and interpretation of the observed optical, electrical and structural properties, Adv. Phys. **18**, 193 (1969).

[41] E. O. Kane, Zener tunneling in semiconductors, J. Phys. Chem. Solids **12**, 181 (1960).
[42] W. Kuehn, P. Gaal, K. Reimann, M. Woerner, T. Elsaesser, and R. Hey, Terahertz-induced interband tunneling of electrons in GaAs, Phys. Rev. B **82**, 075204 (2010).
[43] H. Nishidome, K. Nagai, K. Uchida, Y. Ichinose, Y. Yomogida, Y. Miyata, K. Tanaka, and K. Yanagi, Control of high-harmonic generation by tuning the electronic structure and carrier injection, Nano Lett. **20**, 6215 (2020).
[44] C. H. Lui, K. F. Mak, J. Shan, and T. F. Heinz, Ultrafast photoluminescence from graphene, Phys. Rev. Lett. **105**, 127404 (2010).
[45] W.-T. Liu, S. W. Wu, P. J. Schuck, M. Salmeron, Y. R. Shen, and F. Wang, Nonlinear broadband photoluminescence of graphene induced by femtosecond laser irradiation, Phys. Rev. B **82**, 081408(R) (2010).
[46] S. Ono, Thermalization in simple metals: Role of electron-phonon and phonon-phonon scattering, Phys. Rev. B **97**, 054310 (2018).
[47] S. Ono and T. Suemoto, Ultrafast photoluminescence in metals: Theory and its application to silver, Phys. Rev. B **102**, 024308 (2020).
[48] S. Ghimire, A. D. DiChiara, E. Sistrunk, P. Agostini, L. F. DiMauro, and D. A. Reis, Observation of high-order harmonic generation in a bulk crystal, Nat. Phys. **7**, 138 (2011).
[49] Y. S. You, D. A. Reis, and S. Ghimire, Anisotropic high-harmonic generation in bulk crystals, Nat. Phys. **13**, 345 (2017).
[50] H. Liu, Y. Li, Y. S. You, S. Ghimire, T. F. Heinz, and D. A. Reis, High-harmonic generation from an atomically thin semiconductor, Nat. Phys. **13**, 262 (2017).
[51] F. Langer, M. Hohenleutner, U. Huttner, S. W. Koch, M. Kira, and R. Huber, Symmetry-controlled temporal structure of high-harmonic carrier fields from a bulk crystal, Nat. Photonics **11**, 227 (2017).
[52] T. T. Luu and H. J. Wörner, Measurement of the Berry curvature of solids using high-harmonic spectroscopy, Nat. Commun. **9**, 916 (2018).
[53] H. Lakhotia, H. Y. Kim, M. Zhan, S. Hu, S. Meng, and E. Goulielmakis, Laser picoscopy of valence electrons in solids, Nature (London) **583**, 55 (2020).
[54] C. P. Schmid, L. Weigl, P. Grössing, V. Junk, C. Gorini, S. Schlauderer, S. Ito, M. Meierhofer, N. Hofmann, D. Afanasiev, J. Crewse, K. A. Kokh, O. E. Tereshchenko, J. Güdde, F. Evers, J. Wilhelm, K. Richter, U. Höfer, and R. Huber, Tunable non-integer high-harmonic generation in a topological insulator, Nature (London) **593**, 385 (2021).
[55] K. Uchida, V. Pareek, K. Nagai, K. M. Dani, and K. Tanaka, Visualization of two-dimensional transition dipole moment texture in momentum space using high-harmonic generation spectroscopy, Phys. Rev. B **103**, L161406 (2021).